Acta Cryst. (1979). A35, 718–727

Electron Diffraction Study of Diffuse Scattering due to Atomic Displacements in Disordered Vanadium Monoxide

BY BJØRN ANDERSSON*

Department of Physics, University of Oslo, Oslo, Norway

(*Received* 11 *October* 1978; *accepted* 12 *February* 1979)

Abstract

The diffuse intensity pattern observed by electron diffraction from $VO_{1.23}$ annealed above the ordering temperature, has been interpreted in terms of short-range-order parameters and by model calculations. Emphasis was put on the ordering of displacements, which gives the major contribution at large scattering angles – a range where the intensity variations at 1 MV are well suited for recording. Through detailed dynamical calculations it is shown that a greatly simplified procedure for calculation of the diffuse intensity is justified when the number and strength of dynamical interactions is moderate. A few displacement parameters were derived through a linear, multiple-regression method. Models for the displacements were based on these results and from information about the ordering of defect tetrahedra. These results agree with previous proposals which indicate large static displacements associated with ordering of defects. Apart from the presence of ⟨100⟩ acoustic phones, the indications of an expansion of the nearest-neighbour distance with a large transverse component were most significant. Such rotation may result from movement of atoms towards selected defect clusters. Model calculations demonstrated that rotated tetrahedra or a zig-zag string of atoms is probable – both fitting well into the assumed surroundings of the clusters.

1. Introduction

Diffuse scattering of electrons is recognized as a useful tool for the study of local order. An extensive and detailed survey of the features of scattering can usually be obtained without the specially prepared single crystals which are needed in X-ray and neutron methods. Of special interest in the present work is the fact that the patterns also extend to quite large values of the scattering variable, particularly when high voltages are employed, that is into a region where the contribution from atomic displacements may be the larger one.

However, the interpretation of the diffuse scattering is impeded by the complexity of electron diffraction, particularly by the strong dynamical interactions which invariably will be present. This can be circumvented in different ways. The more widely used approach is to focus on qualitative or geometrical features. Examples are the Fermi surface imaging (Moss, 1969; Ohshima & Watanabe, 1973), the analytical representation of the shape of patterns due to substitutional order (Sauvage & Parthé, 1972), the analysis of vibrational modes (Komatsu & Teramoto, 1966) and model calculations. Another way is to seek out special cases where the dynamical interactions are tractable or can be neglected, and then work along lines similar to those employed in X-ray and neutron diffraction methods. Such an approach was followed in a previous electron diffraction study of defect ordering in vanadium monoxide (Andersson, Gjønnes & Taftø, 1974)† which we then described in terms of order parameters referred to the structural element in the ordered superstructure, ε ($V_{52}O_{64}$).

The non-stoichiometric vanadium monoxide may serve as a typical example of the application of electron diffraction to defect ordering in inorganic compounds. Substitutional and displacement order occur over a wide composition range within the framework of a defect sodium chloride-type structure. The present investigation is focused on the oxygen-rich end, in which two ordered structures, ε and ε', exist (Andersson & Gjønnes, 1970; Bell & Lewis, 1971). The transition between the two appears to be of the displacive type (Andersson, Gjønnes & Forouhi, 1978).

The strong non-monotonic diffuse scattering observed above the ordering temperature reveals a large degree of short-range order. In the previous study (I) the scattering at intermediate angles ($\sin\theta/\lambda \leq 0{\cdot}3$ Å^{-1}) was analysed in terms of substitutional order; the contribution from atomic displacements was then neglected. As is well known from many X-ray studies of short-range order particularly in binary alloys

* Present address: Central Institute for Industrial Research, Blindern, Oslo.

† Hereafter referred to as (I).

0567-7394/79/050718-10$01.00

(Warren, Averbach & Roberts, 1951; Borie & Sparks, 1971; Gragg & Cohen, 1971), a complete analysis of the scattering must include displacement order. It is desirable, therefore, to incorporate displacement scattering in the electron diffraction study also, particularly in the case of vanadium monoxide where atomic displacements appear to play a conspicuous part in the structure, as is also suggested by the quite large Debye–Waller factor found in later investigations (Høier & Andersson, 1974; Watanabe, Andersson, Gjønnes & Terasaki, 1974; Morinaga & Cohen, 1976).

The purpose of the present investigation is thence to obtain information about the ordering of displacements in $VO_{1\cdot23}$ and its relation to the substitutional order and also to explore the possibility of deducing displacement parameters from electron diffraction. Emphasis is put on exploitation of the outer part of the pattern ($\sin\theta/\lambda > 0{\cdot}3$ Å^{-1}). Preliminary analysis of patterns taken at 1 MV indicated the scattering from displacements to be the major contribution in that region (see Fig. 1). This offers as a starting point the possibility of analysing the displacement contribution separately – which is really the opposite of that in (I) where displacements were neglected – and, of course for handling both contributions in a refining stage. The interpretation is based both on model calculations and on the derivation of displacement ordered parameters from the intensity distribution within selected sections of reciprocal space. The results of the latter analysis serve as a guide for selecting models for local atomic displacements which in turn can be compared with structure elements entering into the ordered structure. The scattering calculations are essentially kinematical; dynamical calculations are introduced as corrections and as a guide to favourable diffraction conditions.

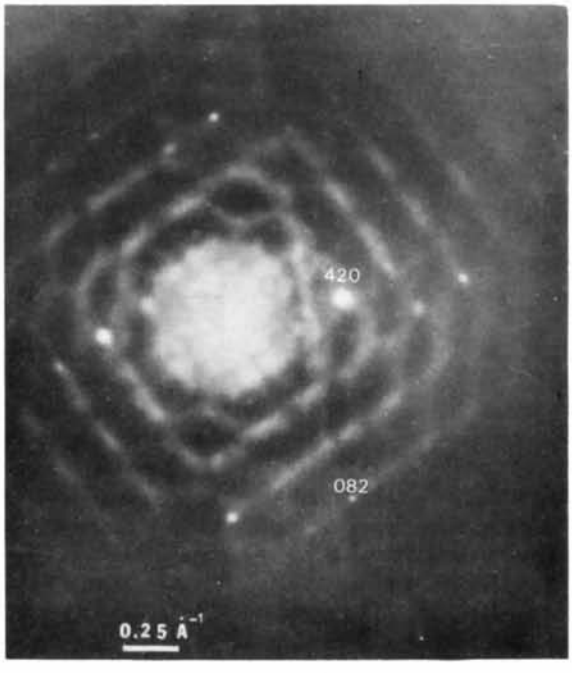

Fig. 1. Diffraction pattern from short-range ordered $VO_{1\cdot23}$ taken at 1 MV with the incident beam nearly parallel to [001]. In the inner part ($\sin\theta/\lambda < 0{\cdot}3$ Å^{-1}) one type of diffuse pattern can be observed which is due to substitutional short-range order of defects. At larger angles a different pattern dominates which is attributed to atomic displacements.

2. Theory – the handling of dynamical interactions

From experimental as well as theoretical studies of diffuse scattering in electron diffraction it emerges clearly that adequate handling of dynamical effects in the patterns is essential. This is especially the case for the displacement type of scattering, which varies both in intensity and qualitative appearance from one Brillouin zone to the next and hence is more susceptible to alterations through Bragg interactions. The magnitude of such effects varies considerably, however. In highly symmetrical projections, like (100), nearly all details may disappear due to dynamical interactions. On the other hand, very distinct patterns can be obtained when only a few Bragg beams are excited. We may take this as an indication that dynamical effects may be tractable.

The aim of this section is to search for conditions where approximate expressions for the diffuse scattering can be shown to be valid. Scattering calculations were based upon a preliminary structure model where four atoms forming the smallest possible tetrahedron were displaced. This model is later shown to be a fair description of the intensity distribution and is expected to bring out the salient features of the dynamical interactions. The calculations were restricted to five interacting beams in order to avoid very long computation times. The projections $(4\bar{1}0)$ and (411) were selected as examples of a favourable case and of one having more pronounced dynamical effects, respectively.

2.1. *Dynamical scattering*

The diffuse scattering of electrons under dynamical conditions is highly complex. Hence, the calculation of the intensity will involve complicated expressions. It is therefore necessary to investigate to what extent simplifications can be made in order to obtain a tractable form of the expressions.

In the present work, these are introduced in the theoretical framework of Gjønnes (1966). The incident electron is considered to be dynamically scattered in the upper part of the crystal, to suffer kinematical diffuse scattering in a thin slice and to be coupled through

Bragg scattering again below that slice. The full expression takes the form

$$I(\mathbf{s}+\mathbf{h}) = \sum_{g}\sum_{g'}\sum_{f}\sum_{f'}\int_{0}^{z} dz_1\, S_{hg}(\mathrm{II})\, S^{*}_{hg'}(\mathrm{II}) \times F^{*}(\mathbf{s}+\mathbf{g}'-\mathbf{f}')\, F(\mathbf{s}+\mathbf{g}-\mathbf{f})\, S_{fo}(\mathrm{I}) \times S^{*}_{f'o}(\mathrm{I}), \qquad (A)$$

where (II) and (I) are substituted for $(\mathbf{k}_0 + \mathbf{s},\ z - z_1)$ and $(\mathbf{k}_0, z_1)$, respectively. $\mathbf{s}$ is a reciprocal vector within the first Brillouin zone, $\mathbf{h}$, $\mathbf{g}$, $\mathbf{g}'$, $\mathbf{f}$ and $\mathbf{f}'$ reciprocal lattice vectors, $\mathbf{k}_0$ the incident scattering vector, z the thickness and z_1 the slice position. F is the function for the kinematical diffuse scattering and S_{fo}, S_{hg} *etc.* those of the dynamical Bragg scattering, *i.e.* elements of the scattering matrix.

The thickness variation within the illuminated area is normally so large compared with the important extinction periods that an average over z appears to be justified. This was also confirmed by calculation of the intensity at selected points in the reciprocal planes for typical thicknesses.

The Bragg scattering between diffuse beams below the slice gives rise to Kikuchi line contrast. In a symmetrical pattern, with the beams along the zone axis, this is to a large extent suppressed. Calculations with and without these terms in the $(4\bar{1}0)$ case indeed reveal small differences in intensity profiles and peak values (Figs. 2*a*,*b*, 4); the significance of these will be discussed in a later section. In the (411) reciprocal plane, on the other hand, the redistribution of diffuse scattering is appreciable (Fig. 3*a*,*b*); here the $S_{hg}S_{hg'}$ terms with $\mathbf{g}, \mathbf{g}' \neq \mathbf{h}$ cannot be neglected even in a qualitative treatment. Hence, care must be taken to select reciprocal planes in which the approximations used are valid.

A further approximation which will facilitate the calculations, is to neglect interference between diffuse beams scattered from different Bragg reflexions, *i.e.* the cross terms with $\mathbf{f} \neq \mathbf{f}'$. This is most easily justified for the monotonic part. Calculations reveal (Figs. 2*c*, 3*c*) only minor contributions also to the non-monotonic part especially in the $(4\bar{1}0)$ plane. Somewhat larger effects are seen in (411), but this is of no practical importance since the previous approximation is too crude anyway.

With these approximations equation *A* for the intensity at $\mathbf{k} = \mathbf{s} + \mathbf{h}$ reduces to:

$$I(\mathbf{k}) = \sum_{f} \langle F(\mathbf{k}-\mathbf{f})\, F^{*}(\mathbf{k}-\mathbf{f})\rangle\, I_f; \quad I_f = S_{of} S^{*}_{of}, \qquad (B)$$

which is really a kinematical intensity distribution, $\langle F(\mathbf{k}-\mathbf{f})F^{*}(\mathbf{k}-\mathbf{f})\rangle$, centred around each Bragg spot $\mathbf{f}$. The scattering factors for the diffuse scattering are

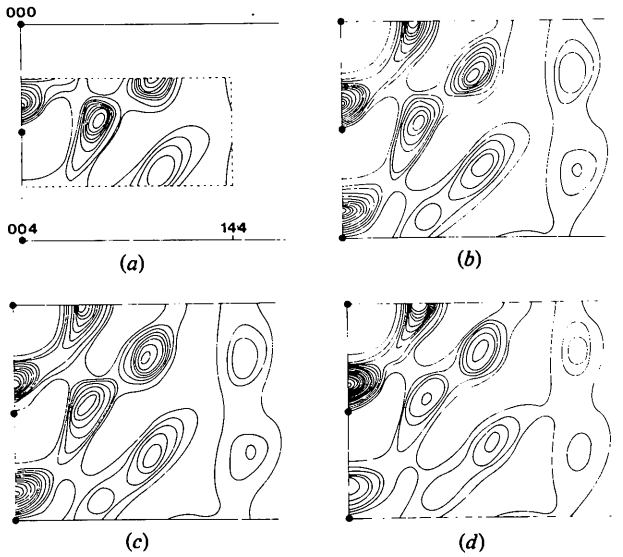

Fig. 2. Theoretical five-beam calculations of the intensity modulations in $4\bar{1}0$ due to ordering of displacements performed with different levels of approximations. (*a*) All interactions kept but thickness averaged. (*b*) Interactions $S_{hg}S^{*}_{hg'}$ above the slice neglected. (*c*) Interface terms $s_{of}S_{of'}$ ($\mathbf{f} \neq \mathbf{f}'$) below the slice neglected. (*d*) All interactions neglected (kinematical case).

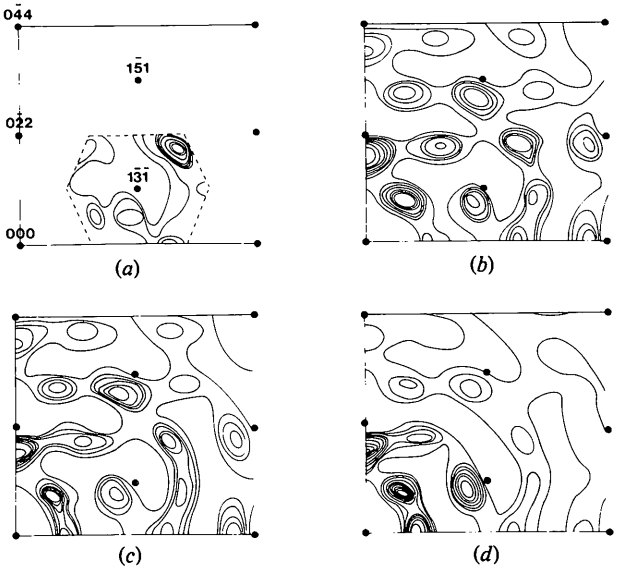

Fig. 3. The same calculation as in Fig. 2 for the (411) plane.

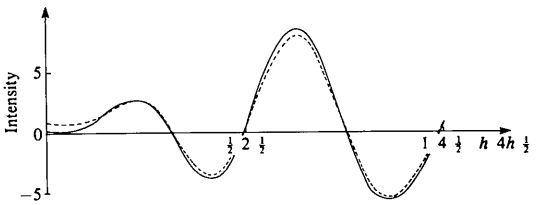

Fig. 4. The calculations shown in Fig. 2 for the line $h4h0{\cdot}5$ displayed as intensity profiles. Full lines correspond to calculations using the full expression and broken lines with $S_{hg}S^{*}_{hg'}$ neglected. The neglect of $S_{of}S_{of'}$ ($\mathbf{f} \neq \mathbf{f}'$) gives an intensity profile very close to the broken line.

included in F and hence given by the different vector $\mathbf{k} - \mathbf{f}$ in each term.

For comparison the purely kinematical patterns (Figs. 2*d*, 3*d*) are also calculated. It can be seen that even in the quite favourable (4$\bar{1}$0) case the intensity values differ considerably, although a qualitative comparison may still be relevant.

Even in the full expression (equation *A*) multiple scattering is not included. Multiple scattering certainly affects the monotonic background even for quite thin crystals. In thicker crystals anomalous absorption gives rise to channelling contrast which has to be avoided. A full treatment of anomalous absorption and multiple scattering is quite complicated, see Høier (1973).

We can thus conclude at this stage, that by selecting appropriate sections of reciprocal space and thin parts of the crystal, the dynamical interactions can be suppressed to an extent which makes quantitative comparisons between experimental and calculated non-monotonic scattering meaningful, even in the case of the displacement type of diffuse scattering. Dynamical calculations can then eventually be introduced as a correction or in the estimation of errors.

2.2. *Kinematical diffuse scattering*

Let us now briefly introduce the kinematical expressions needed in equation *B*, following the original derivation by Borie & Sparks (1971). In an extension to the case of multiple sublattices made by Hayakawa & Cohen (1975) the expressions are:

$$I_d/I_{\mathrm{LM}} = \sum_{lmn} \alpha_{lmn} A_{lmn} + \sum_{p=1}^{3} Q^p h_p + \sum_{p=1}^{3} R^p h_p^2 + \sum_{p=1}^{3} S^{p,p+1} h_p h_{p+1}, \qquad (C)$$

$$Q^p = i \sum_{lmn} \bar{\gamma}^p A_{lmn}, \quad R^p = \sum_{lmn} \bar{\delta}^p A_{lmn}$$

and

$$S^{p,p+1} = \sum_{lmn} \varepsilon^{p,p+1} A_{lmn},$$

where I_{LM} is the Laue monotonic scattering, p indicates the component in the reciprocal coordinate. The components in reciprocal space are h_1, h_2 and h_3 and the indices for interatomic vectors are l, m and n. As usual in work on diffuse scattering, these are twice the indices of the correct Bravais unit cell. A_{lmn} is $\exp[2\pi i(h_1 l + h_2 m + h_3 n)]$. The zero-order contribution will be called I_{SRO} and sum of higher order I_{DIS}. I_{LM} will be included in these contributions.

It should be noted that the squares of the individual displacements which would have entered into even orders in the expansion, are collected into a temperature-factor-like expression. This is included in the scattering factors. The parameters $\bar{\alpha}$, $\bar{\gamma}$, $\bar{\delta}$ and $\bar{\varepsilon}$ are to be determined. A given interatomic vector will, since there are several sublattices, connect unlike pairs of atoms. There are three types of vectors: (1) between atoms on the same f.c.c. sublattice, (2) between the metal and the oxygen lattice and (3) between the f.c.c. and the tetrahedral sublattices. A parameter can be assigned to a vector connecting pairs of atoms on the same sublattice, but only the sum of such parameters having the same interatomic vector can be determined in a kinematical experiment.* This sum (or average) is indicated by a bar over the parameter symbols.

By inserting the expressions I_{SRO} and I_{DIS} into the dynamical equation (*C*) the following modification to the substitutional and displacement contribution is obtained:

$$I'_{\mathrm{SRO}}(\mathbf{k}) = \sum_f I_{\mathrm{SRO}}(\mathbf{k} - \mathbf{f}).I_f$$

and

$$I'_{\mathrm{DIS}}(\mathbf{k}) = \sum_f I_{\mathrm{DIS}}(\mathbf{k} - \mathbf{f}).I_f. \qquad (D)$$

3. Experimental

Preparations and thinning of samples for studies in the electron microscope have been described in earlier investigations (Andersson & Gjønnes, 1970) and in (I). Diffraction patterns were recorded photographically at 1 MV and 100 kV using JEOL-1000 and Phillips EM 300 microscopes, respectively. The photographic plates were photometrically analysed in scans and numerical values obtained for the intensity. Each scan has a width of $\Delta h \simeq 0{\cdot}05$ reciprocal lattice units. The uncertainty in position determination was about 0·01. Considering the noise level and technique of measurement, the uncertainty in the intensity values is estimated to be $\simeq 1$ on the scale chosen.

4. Results

Electron diffraction patterns taken from the thin part of each specimen show strong diffuse scattering with intensity variations extending to about $\sin\theta/\lambda = 1$ Å^{-1} at 1 MV (Fig. 1). Patterns taken at 100 kV have the same general appearance, but have comparable contrast only to about 0·5 Å^{-1} in that case. The complete patterns can be divided into two types which dominate at low and high scattering angles respectively.

The inner part of the diffuse pattern ($\sin\theta/\lambda \lesssim 0{\cdot}3$ Å^{-1}) which was analysed in (I), is characterized by the repetition of the shape of the pattern with the Brillouin zone. This type therefore lends itself readily to interpretation in terms of substitutional short-range order.

* Information about single parameters may in principle be obtained in dynamical experiments.

The outer pattern cannot be regarded as an extension of the inner one, but as a distinctly different type. The most conspicuous features can be described schematically in terms of diffuse {100} intensity walls positioned slightly outside $2kl$, $4kl$, $6kl$ *etc.* in a sector around ⟨100⟩ directions. The walls are closer to $h = 6$ than to $h = 2$. The intensity is weakened where the walls are closest to the reciprocal lattice points. The shape changes gradually with the direction of the scattering vector and becomes cellular-like between the ⟨100⟩ directions.

The intensity variations are clearly associated with displacement order. This follows from the change in the pattern from one Brillouin zone to the next, especially with the direction of the scattering vector **s**, the fact that this type of pattern shows maximum contrast at some finite angle and falls off rather slowly towards higher $|\mathbf{s}|$ values and the slight shift of the position of the intensity walls with $|\mathbf{s}|$. All of these features can be related to the prefactors of type $(\mathbf{s}.\boldsymbol{\Delta})$, $(\mathbf{s}.\boldsymbol{\Delta})^2$ *etc.* ($\boldsymbol{\Delta}$ is a displacement vector) in the displacement terms.

These qualitative considerations together with a later calculation of the different contributions (Fig. 8) demonstrate that the substitutional short-range-order contribution is negligible at large scattering angles. The opposite is not so obvious at low angles. The weaker and much more slowly varying intensity due to displacements makes it, however, easy to separate the contribution qualitatively.

We have thus seen that the large range of scattering variables available in the electron diffraction case, particularly at 1 MV, allows a separation of substitutional and displacement order contributions, at least in a qualitative sense. This is clearly an advantage compared with most X-ray and neutron diffraction studies (Borie & Sparks, 1971). It may be hoped that this advantage will to some extent compensate for the less precise theoretical description. The drawbacks of such an approach are the difficulties in obtaining absolute values, normalizing between different reciprocal planes and utilizing large portions of the reciprocal space.

All considered, it was found worthwhile to attempt a description of the intensity distribution, using either models for local displacements, or intensity expressions based upon expansions in displacement parameters. But first an expression for the structure-independent background had to be determined.

4.1. *Background*

Adequate expressions for the contributions to the smooth background like the phonon and plasmon scattering do not exist. Furthermore, a proper handling of multiple diffuse scattering is not feasible. Therefore an empirical expression has to be introduced. This must include inelastic scattering and monotonic terms in I_{SRO} and I_{DIS}. Several mathematical forms were tried such as power series and one or several Gaussian distributions. It was found best, however, to plot the intensity *versus* scattering variables in a number of representations in order to derive a suitable form. This was done in a region where the scattering around the strong central beam dominates; the line $h4h0$ in $(4\bar{1}0)$ was selected. A plot of the intensity on a logarithmic scale against $\sin\theta/\lambda$ gave a linear dependence between 0·2–0·75 $Å^{-1}$ changing to a steeper slope at high angles (Fig. 5). A fair representation of the background was obtained with the function $A\exp[-W(\sin\theta/\lambda)]$ where the width parameter W is changed at $\sin\theta/\lambda \gtrsim 0{\cdot}75$ $Å^{-1}$; a second exponential of much shorter width was included, which is important only close to the Bragg peaks.

4.2. *Non-monotonic intensity variations*

The two reciprocal planes $(4\bar{1}0)$ and $(7\bar{8}5)$ with symmetrical incidence (Fig. 6) were chosen principally from consideration of the dynamical interactions as discussed in § 3. The photometric curves taken in $(4\bar{1}0)$ are shown in Fig. 7. Several areas have to be excluded within the measured part of the reciprocal plane in the fitting procedure.

These were: (i) the areas where diffuse scattering due to substitutional order is appreciable; (ii) the areas close to Bragg peaks where the description of background intensity is inadequate and (iii) the areas at the largest diffracting angles where the non-monotonic intensity contribution is very low. The remaining area which is shown hatched in Fig. 7(*b*) in the case of $(4\bar{1}0)$, still includes the most important features of the displacement contribution to the diffuse scattering.

The non-monotonic intensity within this region was analysed in terms of displacement parameters using a

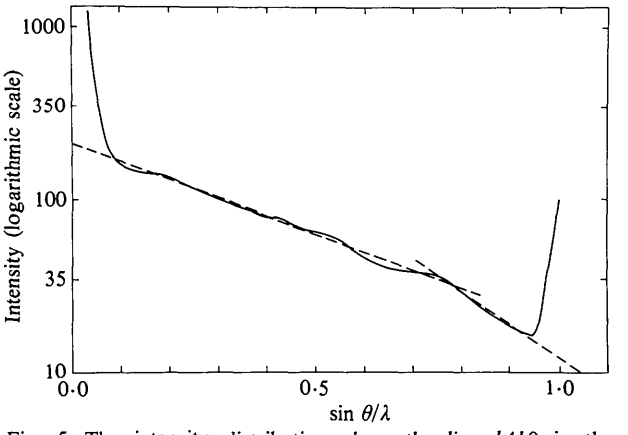

Fig. 5. The intensity distribution along the line $h4h0$ in the reciprocal plane $(4\bar{1}0)$ drawn with full lines on a logarithmic scale against $\sin\theta/\lambda$. Broken lines indicate the empirical background contribution.

linear least-squares method. The number of parameters was therefore kept low by incorporating larger vectors stepwise while excluding parameters of insignificant values. As it turned out that interatomic vectors larger than about ⟨220⟩ have little importance, these were neglected. The final number of parameters became 21 after also omitting contributions from the V–O distance ⟨210⟩ and keeping only the cross term in ⟨220⟩.

Adjustable parameters entering into the expressions, *viz* the width of the background intensity distribution, the temperature factor and the intensity of the central peak, were varied to the best fit.

As a final refinement, the neglected moments in the series expansion of the diffuse scattering were included. The substitutional short-range-order scattering I'_{SRO} was calculated from the results obtained in (I) and subtracted: this had negligible effect, however. Incorporation of higher-order terms – calculated with equations given by Hayakawa & Cohen (1975) – slightly improved the fit. The fitting procedure was rerun after subtraction at the third- and fourth-order contribution; the results are shown in Table 1.

The average errors in intensity are about 1·4 and 1·8 in the two fits in $(4\bar{1}0)$ and $(7\bar{8}5)$, respectively. This is about twice the standard deviation of the measurements and consequently systematic errors are indicated. Deliberate changes in the adjustable param-

Table 1. *Experimental results for displacement parameters*

Displacement parameters	Least-squares results from $4\bar{1}0$	from $7\bar{8}5$	Weighted average	Errors due to misfit
δ^x_{110}	2·4	2·0	2·2	0·1
$\delta^y_{100} = \delta^z_{100}$	−0·1	−0·4	−0·2	0·1
$\gamma^x_{110} = \gamma^y_{110}$	6·0	7·1	6·7	0·5
$\delta^x_{110} = \delta^y_{110}$	−0·24	−0·12	−0·20	0·04
δ^z_{110}	0·28	0·16	0·25	0·08
ε^{xy}_{110}	−1·3	−0·9	−1·1	0·12
$\delta^x_{111} = \delta^y_{111} = \delta^z_{111}$	0·2	0·03	0·12	0·04
$\varepsilon^{xy}_{111} = \varepsilon^{yz}_{111} = \varepsilon^{xz}_{111}$	−0·3	−0·3	−0·3	0·1
γ^x_{200}	−2·5	−6·6	−4·0	1·1
δ^x_{200}	0·48	0·16	0·35	0·08
$\delta^y_{200} = \delta^z_{200}$	−0·16	−0·16	0	0·08
γ^x_{211}	−0·9	−0·7	0	0·6
$\gamma^y_{211} = \gamma^z_{211}$	−0·4	−1·0	−0·6	0·3
δ^x_{211}	0·12	0·06	0·10	0·04
$\delta^y_{211} = \delta^z_{211}$	0·06	0·14	0	0·03
$\varepsilon^{xy}_{211} = \varepsilon_{211}$	0·3	0·12	0·20	0·08
ε^{yz}_{211}	0·12	0·44	0·20	0·08
ε^{xy}_{220}	0·52	0·12	0·35	0·24

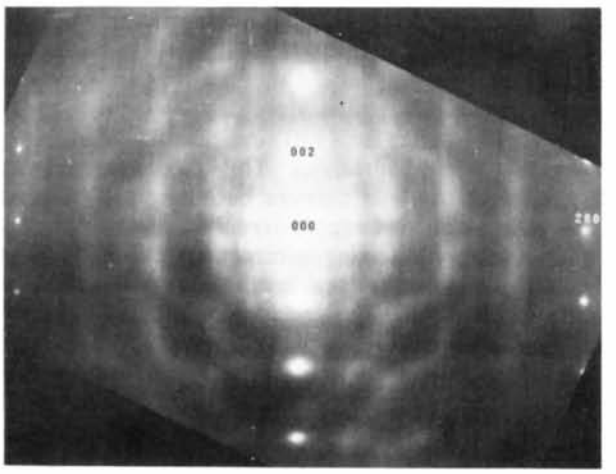

(*a*)

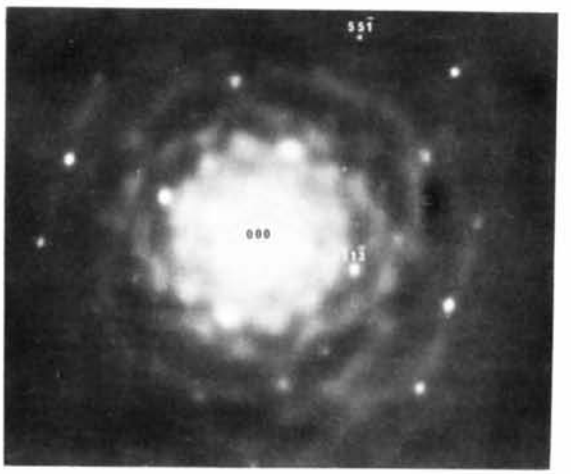

(*b*)

Fig. 6. The reciprocal planes (*a*) $(4\bar{1}0)$ and (*b*) $(7\bar{8}5)$ which are utilized for determinations of the displacement parameters.

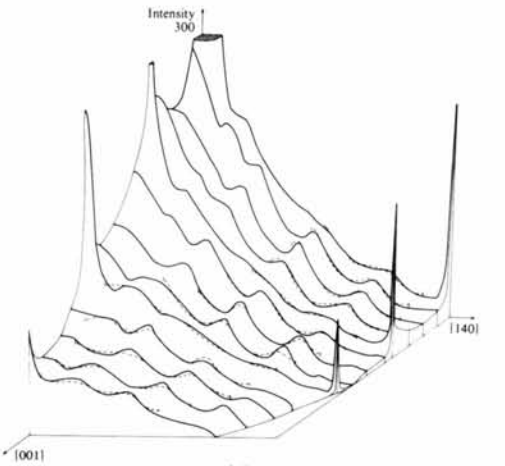

(*a*)

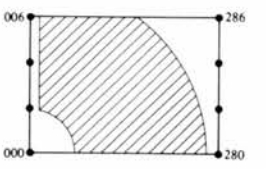

(*b*)

Fig. 7. (*a*) Photometer traces in the $(4\bar{1}0)$ reciprocal plane along lines parallel to [140]. (*b*) The area where measurements are carried out. Values used for the least-squares fit are within the hatched area.

eters and refinements in the calculation were made to estimate resulting deviations in the parameter values. These were found to be small, however, compared with the scatter in the determined parameter values. The correlations between parameters were calculated and estimated to be small in both planes. Furthermore, the simplifications in the theory lead to deviations in the intensity profiles which are smaller or comparable with the uncertainty in the measurements (Fig. 3) and hence are of little importance at the present stage. It is therefore felt that the main uncertainty arises from the methodological problem of using few parameters, small portions of reciprocal space and errors in the background correction. Some of these errors will be compensated in a fit in one plane. It is estimated that the uncertainties are about two to three times those obtained in one plane (Table 1).

4.3. *Normalization*

Normalization of the diffuse scattering, in order to obtain absolute size of the displacements, is usually carried out by relating the non-monotonic terms to the background. This is not possible in the present case. In order to obtain an approximate normalization, the displacement contribution was compared with the substitutional part. The justification for this procedure lies in the fact that I_{SRO} peak values are given to a large degree by the self correlation term, *i.e.* more by the number of tetrahedral clusters which is quite well determined than by the more uncertain α parameters.

Table 2. *Normalized displacement parameters* ($\times 10^3$)

Inter-atomic vector	First order			Second order					
$\{lmn\}$	γ^x	γ^y	γ^z	δ^x	δ^y	δ^z	ε^{xy}	ε^{xz}	ε^{yz}
100				62	6	6	0	0	0
110	186	186	0	−6	−6	7	−32	0	0
111				4	4	4	9	9	9
200	−110	0	0	11	0	0	0	0	0
211	(−21)	(−17)	(−17)	3	(3)	(3)	5	5	5
220							(8)		

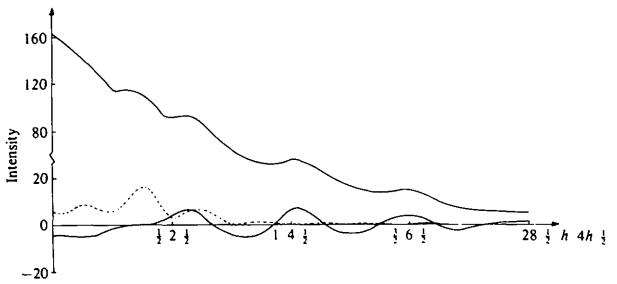

Fig. 8. The measured intensity profile along $h4h0{\cdot}5$ in $(4\bar{1}0)$ shown together – in the double scale – with the substitutional short-range order contribution I'_{SRO} (broken line) and the displacement contribution I'_{DIS} (full line). I'_{SRO} is calculated from (I) and the derived proportional factor.

The line $h4h0{\cdot}5$ which passes through maximal intensity variation of both I'_{SRO} and I'_{DIS} was chosen for this purpose. The theoretical I'_{SRO} was fitted to the experimental one (Fig. 8). A proportional factor was obtained which was used for relating parameter values to absolute units. The relative uncertainty in the factor is estimated to about 30%. The normalized parameters are shown in Table 2.

4.4. *Interpretation of the parameters and model calculations*

The displacement parameters obtained above were used to construct models for the atomic displacements. Such models have to be consistent with the local order of defect tetrahedra revealed by earlier studies of the diffuse scattering at lower angles. It is expected that the metal atoms will be displaced towards neighbouring vacancies. Taking the ordered $V_{52}O_{64}$ as an example, one finds that the metal atoms will have two, three or four vacancies as neighbours which will belong to two different clusters (I). Similar configurations around metal atoms appear likely also for other reasonable intercluster vectors such as those which are probable above the transition temperature (I).

The γ parameters for $\langle 110 \rangle$ indicate an expansion of nearest-neighbour distances. This is consistent with displacement towards clusters because $\langle 110 \rangle$ atomic pairs normally lie between different tetrahedra (Fig. 9). Other γ values indicating contractions call for a more detailed model for the local arrangement. However, for a cluster arrangement resembling the ordered structure and with the same type of displacement as suggested for $\langle 110 \rangle$ pairs, the contractions appear reasonable.

The interpretation of second-order parameters is complicated by the contribution from thermal vibrations. In a perfect NaCl-type structure these are

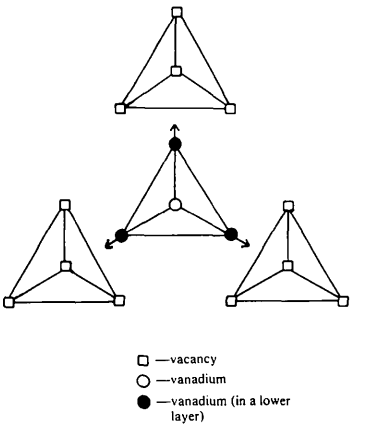

Fig. 9. A local arrangement of defect tetrahedra separated by $\langle 220 \rangle$ distances, seen along a $\langle 111 \rangle$ axis. Atoms in the centre tetrahedron (on a lower level) can displace towards selected clusters as indicated by the arrows.

expected to give {100} intensity walls and weaker {110} walls (Lonsdale & Smith, 1941; Honjo, Kodera & Kitamura, 1964) which will yield large contributions to δ^x_{h00}. Assuming that the modes of thermal motion are not drastically altered by the presence of defects, it appears reasonable to relate part of the large value for δ^x_{100} to thermal vibrations, notably to acoustic phonons with the polarization vector along [100]. The second-order parameters for other distances are of a magnitude which is consistent with the values of the first-order parameters. The large negative cross term ε^{xy}_{110} appears to be of particular structural interest. This parameter means that the ⟨110⟩ pair expand without any rotation. The quadratic terms indicate that the respective products of x, y and z displacement components of the two atoms are all very small.

Some simple atomic configurations have been constructed on the basis of the information in these parameters. As examples were chosen (see Fig. 10): pair, triangle, square and tetrahedron of atoms; all with ⟨110⟩ edges. A large cluster, where the nearest neighbour to a defect tetrahedron is displaced inwards, was also included.

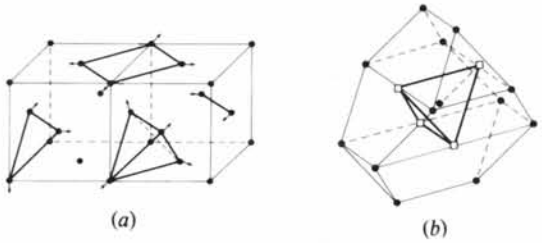

Fig. 10. (*a*) Displacement models with two, three and four atoms. (*b*) Nearest neighbours to a defect tetrahedron. Displacements are either towards the centre or the two nearest vacancies.

Starting with a single ⟨110⟩ pair, displacements along [0$\bar{1}$0] and [100] of the respective atoms yield an expansion, no quadratic terms and a large negative cross term. Since the triangle can be composed of such pairs, the same intensity pattern will be the result. Displacements of directions ⟨311⟩ which will point towards a neighbouring defect tetrahedron, have therefore been tested. The square can also be composed of preferable ⟨110⟩ pairs but the ⟨200⟩ pair will be distorted in a wrong way. For the tetrahedron model a pure expansion offers the best compromise. Quadratic terms will be larger than expected, however.

As seen from Fig. 11, all models except the square and the large cluster yield satisfactory agreement with experimental diffuse intensity patterns. In the first case the disagreement can be attributed to the incorrect displacements of ⟨200⟩ pairs. The very poor agreement obtained with the large cluster (Fig. 11*f*) demonstrates that the metal displacements are not governed by a single defect tetrahedron. An interpretation must therefore invoke several clusters as expected.

To see how the preferable models can be incorporated into the structure, an idealized local arrangement of defect tetrahedra is taken as a starting point. Since the most preferable intercluster distances are centred around 220, typical surroundings of the metal atoms will be as shown in Fig. 9. If the atoms are allowed to shift towards selected defect clusters in ⟨100⟩ or ⟨311⟩ directions, both the pair and the tri-

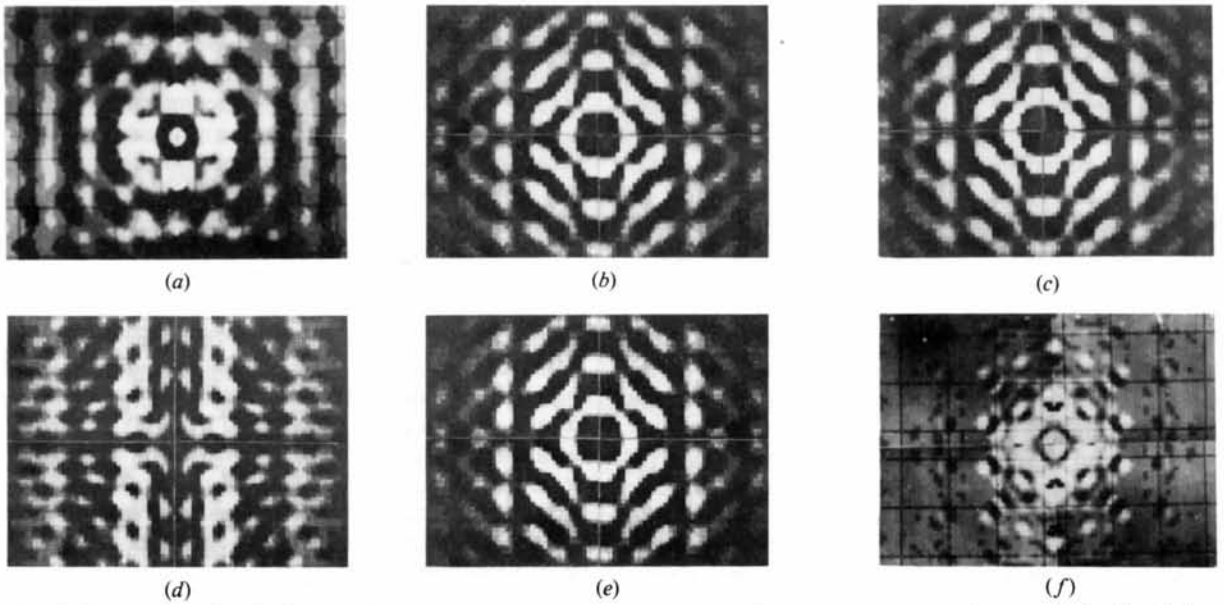

Fig. 11. Calculated intensity distributions with the background subtracted. The substitutional short-range order contribution is calculated from Andersson *et al.* (1974). Calculations are based on (*a*) experimental displacement parameters and models forming (*b*) pairs, (*c*) triangles, (*d*) squares, (*e*) tetrahedra, and (*f*) closest neighbours to the defect cluster.

angle model will result. Also the tetrahedron model can be approximated or regarded as a sort of average structure element.

These considerations can only to a degree be carried over to the ordered structure. An expansion of ⟨110⟩ pairs towards a selected tetrahedron is reasonable in this case as well. However, in view of the symmetry of the structure, a rotation component is expected.

5. Discussion

Part of the present investigation has been concerned with the problem of handling the dynamical interactions theoretically and experimentally, in order to obtain meaningful results from the analysis of electron diffraction patterns. The best way of handling these interactions (equation *A*) is to reduce the number and excitation of beams. By careful analysis of dynamical effects it is possible to find projections where a near kinematical approach (equation *B*) is justified. In such cases, the approximations used lead only to minor changes in the calculated intensity values. In other cases where more Bragg beams are more strongly excited – like in the (411) case – such an approach cannot be used.

Anomalous absorption and multiple diffuse scattering raise additional problems. At present, these can only be handled by selecting patterns taken from thin parts of the specimen. A theoretical analysis of these effects and the influence of the parameters has not yet been attempted.

The difference between experimental and calculated intensity distributions indicates systematical errors to be present. Inadequate handling of the dynamical interactions is not felt to be a major contributing factor to this (Figs. 2, 3, 4). Rather, uncertainties arise due to the common problem in regression analysis like those connected with the limited set of parameters, slightly wrong fixed parameters and the choice of data. Additional problems arise in the present case, due for instance to the limitations in the choice of reciprocal planes and of range of scattering variables and due to errors in background and in intensity expressions. In the linear-regression analysis it is difficult to trace the origin of the errors, as these will, as always in such analyses, to some extent be compensated for in the fitting procedure. It appears, however, that a few parameters may be meaningful.

The method of separating the two contributions I'_{SRO} and I'_{DIS} by simply studying each of them in selected regions of the reciprocal space seems to be valid in the case of I'_{DIS} (see Fig. 8). The I'_{SRO} contribution can be distinguished qualitatively by means of the greater sharpness and the different features of the patterns. In this case it can be noted that dynamical interactions may facilitate the interpretation. This stems from the fact that dynamical interactions tend to reorganize I_{DIS} but not I_{SRO}. As a limiting case when several strong beams are excited, the first type of pattern can be completely smeared out. This was indeed confirmed by the calculations in the area inside $1\bar{3}\bar{1}$ in (411), where most interactions are effective in the five-beam case considered. Thus in this area, which was studied earlier (I), it is expected that I'_{DIS} will be smeared out but I'_{SRO} will remain with some change in intensity.

It may be of interest to compare the parameter errors associated with different diffraction methods. Unfortunately these are not easily obtained in the widely used Fourier analysis, but estimates of 20–50% in the α parameters are quoted (Hayakawa, Bardhan & Cohen, 1975) when the size terms are large and the Borie & Sparks (1971) method is employed. The errors in the displacement parameters will certainly be even higher. Consequently, the present method may yield results up to the same level as a conventional X-ray experiment under these unfavourable conditions. This may appear somewhat surprising in view of the theoretical difficulties, but can be attributed to the larger intensity variations available and the lower background intensity in the electron diffraction case. It must be noted, however, that an X-ray experiment can be improved with newer methods and the calculations can be refined. The uncertainties can thereby be reduced by an order of magnitude in favourable cases. Thus, a study of displacement ordering should definitely be performed by X-ray methods if suitable crystals are available.

Despite the difficulties and inaccuracies experienced with the electron diffraction method it seems fair to say that the method may be used for determination of order parameters. The advantages of the method are the wide applicability and the ease with which data can be obtained. Thus in many cases electron diffraction may be the only method capable of giving information about the short-range ordering of displacements.

The parameters found in the present investigation show that atomic displacements constitute an important element in the local order in the system, as already indicated by the large values of the Debye–Waller factor obtained previously (Watanabe *et al.*, 1974; Morinaga & Cohen, 1976). The normalized values for the parameters indicate that about one half of the *B* factor can be associated with static displacements or rather displacements connected with the defect ordering. The detailed local arrangement responsible for the atomic shifts, can be interpreted in terms of the defect tetrahedra which occur in the disordered as well as the ordered structure. The salient feature of displacement ordering is found to be a nearly transverse expansion of the nearest-neighbour metal–metal distance. This can be explained by assuming the metal atoms to be shifted towards different neighbouring defect tetrahedra in a way which is consistent with the short-range order of tetrahedral defects found previously (I). It can be seen

that the transition between the two ordered phases ε and ε' also appears to be connected with atomic displacements (Andersson *et al.*, 1978) which thus seem to play a significant part in the structural behaviour of the system.

References

ANDERSSON, B. & GJØNNES, J. (1970). *Acta Chem. Scand.* **24**, 2250–2252.

ANDERSSON, B., GJØNNES, J. & FOROUHI, R. (1978). *J. Less-Common Met.* **61**, 273–291.

ANDERSSON, B., GJØNNES, J. & TAFTØ, J. (1974). *Acta Cryst.* A**30**, 216–224.

BELL, P. S. & LEWIS, M. H. (1971). *Phys. Status Solidi A*, **7**, 431–439.

BORIE, B. & SPARKS, C. J. (1971). *Acta Cryst.* A**27**, 198–201.

GJØNNES, J. (1966). *Acta Cryst.* **20**, 240–249.

GRAGG, J. E. & COHEN, J. B. (1971). *Acta Metall.* **19**, 507–519.

HAYAKAWA, M., BARDHAN, P. & COHEN, J. B. (1975). *J. Appl. Cryst.* **8**, 87–95.

HAYAKAWA, M. & COHEN, J. B. (1975). *Acta Cryst.* A**31**, 635–645.

HØIER, R. (1973). *Acta Cryst.* A**29**, 663–672.

HØIER, R. & ANDERSSON, B. (1974). *Acta Cryst.* A**30**, 93–95.

HONJO, G., KODERA, S. & KITAMURA, N. (1964). *J. Phys. Soc. Jpn*, **19**, 351–367.

KOMATSU, K. & TERAMOTO, K. (1966). *J. Phys. Soc. Jpn*, **21**, 1152–1159.

LONSDALE, K. & SMITH, H. (1941). *Proc. R. Soc. London Ser. A*, **179**, 8–50.

MORINAGA, M. & COHEN, J. B. (1976). *Acta Cryst.* A**32**, 387–395.

MOSS, S. C. (1969). *Phys. Rev. Lett.* **22**, 1108–1111.

OHSHIMA, K. & WATANABE, D. (1973). *Acta Cryst.* A**29**, 520–526.

SAUVAGE, M. & PARTHÉ, E. (1972). *Acta Cryst.* A**28**, 607–616.

WARREN, B. E., AVERBACH, B. L. & ROBERTS, B. W. (1951). *J. Appl. Phys.* **22**, 1493–1496.

WATANABE, D., ANDERSSON, B., GJØNNES, J. & TERASAKI, O. (1974). *Acta Cryst.* A**30**, 772–776.

Acta Cryst. (1979). A**35**, 727–732

Calculation of Coulombic Energy for Molecular Crystals

BY CARLO MARIA GRAMACCIOLI AND GIUSEPPE FILIPPINI

Istituto di Chimica Fisica e Centro CNR, Università, via Golgi 19, *I* 20133 *Milano, Italy*

(*Received* 22 *December* 1978; *accepted* 20 *March* 1979)

Abstract

The first Bertaut series has been examined for practical application to evaluating coulombic contribution to lattice energy in molecular crystals; especially with Templeton's correction, its use seems to be quite advantageous because of its simplicity and does not seem to involve a longer computing time than other methods. For rigid molecules, a scheme of obtaining first and second derivatives of coulombic energy with respect to molecular rotation or translation is shown; this scheme can be easily applied to packing energy minimization and also to constrained refinement of crystal structures.

Introduction

Calculation of various properties in molecular crystals by packing analysis seems nowadays to be a quite well-established routine, which affords promising applications in obtaining, for instance, vibrational data, temperature factors and even thermodynamic functions connected with the second law, such as entropy, free energy, *etc.*, or in the field of surfaces.

In our treatment of several 'rigid' molecules (Filippini, Gramaccioli, Simonetta & Suffritti, 1973, 1974*a*,*b*, 1975*a*,*b*, 1976, 1978), we have excluded coulombic interactions so far; however, in many cases they cannot be neglected, especially when polar molecules are dealt with, and even for 'ordinary' hydrocarbons the introduction of charge effects seems to lead to a definite improvement (Warshel & Lifson, 1970; Williams, 1974).

For molecular crystals, three points are particularly important. The first is connected with the possibility of easy minimization of packing energy by some automatic routine, so that comparison between the packing conformations calculated from different potential functions becomes possible, and also a starting point for lattice-dynamical calculations is obtained (Pawley, 1967); for this reason, if the calculation of derivatives with respect to molecular coordinates (positional and orientational) in the unit cell is easy and fast, this may become an essential advantage. The second point is

0567-7394/79/050727-06$01.00